Influence of Bio-Inspired Ag doped MoO3 Nanoparticles in the Seedling Growth and Inhibitory Action Against Microbial Organisms

A. Nirmal Paul Raj
Research Department of Chemistry, St. John's College
R. Biju Bennie
Research Department of Chemistry, St. John's College
G. Alex Immanuel Xavier
Research Department of Chemistry, St. John's College
C Joel
Research Department of Chemistry, St. John's College
D. Abiya Chelliah
Affiliated to Manonmaniam Sundaranar University
S. Hari Kengaram (harikengaram2009@gmail.com)
PMT college https://orcid.org/0000-0003-4226-244X

Research Article

Keywords: Nanoparticles, MoO3, Band gap energy, Antimicrobial studies, Seed germination

Posted Date: June 7th, 2021

DOI: https://doi.org/10.21203/rs.3.rs-571730/v1

Influence of Bio-inspired Ag doped MoO_3 nanoparticles in the seedling growth and inhibitory action against microbial organisms

A. Nirmal Paul Raj[1a], R. Biju Bennie[1], G. Alex Immanuel Xavier[1], C. Joel[1b,*], D. Abiya Chelliah[2], S. Hari Kengaram[3,*]

[1a]Research Scholar (Reg. No.18221272031022) & Assistant Professor, Research Department of Chemistry, St. John's College, Palayamkottai-627002, Tirunelveli, Tamil Nadu, India.

[1b]Assistant Professor, Research Department of Chemistry, St. John's College, Palayamkottai-627002, Tirunelveli, Tamil Nadu, India.

[2]Research Department of Botany, St. John's College, Tirunelveli-627002, Tamil Nadu, India.

[3]Associate Professor, Department of Chemistry, PMT College, Melaneelithanallur-627953, Tamil Nadu, India.

[1,2,3]Affiliated to Manonmaniam Sundaranar University, Abishekapatti, Tirunelveli-627012, Tamil Nadu, India.

Abstract

Herein we report the hydrothermal synthesis, characterization and biological applications of h-MoO_3 and silver doped MoO_3 nanoparticles (NPs). The phase formation of the synthesized NPs was identified using X-ray diffraction studies and vibrational spectral studies. The average crystallite size of the NPs tends to decrease as the dopant concentration increases. The surface morphology and the elemental composition of the nanoparticles were observed from SEM and EDAX analysis. The crystallite nature was obtained from HRTEM images. The band gap energies obtained from UV-DRS spectra for h-MoO_3 (3.26 eV) were starting to decrease as the concentration of the dopant Ag increases (3.22-2.76eV). The antibacterial activity of the prepared nanoparticles was tested against some gram positive and gram negative bacterial strains *viz., Staphylococcus aureus, Bacillus cereus and Citrobacter koseri* and *Pseudomonas aeruginosa respectively*. Also their seed germination properties were studied on foxtail and finger millet seeds for a period of seven days.

Keywords: Nanoparticles; MoO_3; Band gap energy; Antimicrobial studies; Seed germination

Corresponding authors:

Dr. S. Hari Kengaram

E-mail: harikengaram2009@gmail.com

Dr. C. Joel

E-mail: joeldcc@yahoo.co.in

1. Introduction

Agriculture is considered to be the most vital and stable part due to the production of raw materials for food and feed producing industries. In order to meet the demands of the growing population, there is a necessity to enhance the existing food production. The deterioration of natural resources viz., land, water and soil due to contamination claims the need for agricultural development to be economic, viable and eco-friendly [1]. In the existing situation, the agricultural field is prone to irregular climatic changes, contamination of resources by various hazardous pollutants like fertilizers and pesticides which leads to the elevation of food demands for the growing population [2]. Thus, it is known that there is a need for increased crop production as well as better food security.

No doubt that the sustainable growth of agriculture totally depends on the new and innovative techniques like nanotechnology. In agro-industrial sector, nanotechnology is commonly used in the production of herbicides, fertilizers, fungicides, pesticides as well as nano-sensor materials [3]. These advances can be used to overcome the future demands in agriculture thereby increasing quality and yield of crops thus reducing the environmental pollution due to chemicals and also protecting the vegetatation against environmental stresses [4]. The of NPs serve a better application in agricultural filed by reducing the nutrient losses to enhance their yields and minimizing the cost of production to obtain maximum output [5].

The nanoherbicides and nanopesticides used for the treatment of weeds and pests is observed to significantly increase the crop production. Various types of polymeric and inorganic nanoparticles are utilized as nanoherbicides. Nanomaterials having specific antimicrobial properties aid in the prevention of microbial invasions. Using nanotechnology researchers have designed a smart delivery system to release the nutrients to the targeted site in a slow and controlled manner in order to tackle the nutrient deficiency in plants.

Among the transition metal oxides, molybdenum trioxide (MoO_3) has attracted the attention of the researchers greatly on account of its multifunctional structural, optical, electronic properties along with better intercalation chemistry with unique chemical, electrochemical, and catalytic properties. Molybdenum trioxide (MoO_3), an n-type semiconductor material with a wide band gap of 2.8-3.6 eV [6]. There are three common phases of MoO_3: a thermodynamically stable orthorhombic phase (α-MoO_3) and two metastable phases: monoclinic (β-MoO_3) and hexagonal (h-MoO_3) [7]. The hexagonal phase of MoO_3 is composed of the zigzag chains of MoO_6 octahedrons connecting through the cis-positions [8,9]. In addition, MoO_3 was found to be an effective antimicrobial against different bacterial strains [10]. Antimicrobial activity of MoO_3 is related to their acidic surface involving the formation of intermediate molybdic acid [11]. Also, Mo is responsible for the conversion of nitrogen into ammonia (NH_3) and important for the metabolism of nitrogen and sulfur. However, the increased amount of Mo in plants leads to molybdenum toxicity, causing yellowish leaves, reduced growth in seedlings, and increased concentrations of anthocyanin [12].

Silver nanoparticles (AgNPs) are extensively used for their antimicrobial property against a wide range of phytopathogens [13]. Silver nanoparticles can constantly release the silver ions, which may be considered the mechanism behind their antimicrobial effect. Owing to the electrostatic attraction and greater affinity towards sulfur proteins, silver ions can stick to the cytoplasmic membrane of the cell and increase the permeability of the membrane leading to disruption of the bacterial cell [14]. In recent times, silver nanoparticles have been involved in enhancing seed germination, plant growth and improving photosynthetic quantum efficiency and also serve as antimicrobial agents in treating plant diseases. There are many reports showing that AgNPs with appropriate concentrations play a crucial role in enhancing seed germination and plant growth [15].

Owing to the extensive applications of *h*-MoO_3 and Ag nanoparticles, in this study, we report the synthesis of Ag doped *h*-MoO_3 nanoparticles and their characterization using several analytical techniques. The antibacterial studies of these nanoparticles against *Staphylococcus aureus, Bacillus cereus, Citrobacter koseri and Pseudomonas aeruginosa* strains have been evaluated and also their seed germination properties on the seeds of foxtail millet and finger millet seeds have been studied.

2. Materials and methods

2.1 Materials

All the chemicals used in this research work are of analytical grade. Ammonium heptamolybdate tetrahydrate (AHM) was purchased from Sigma Aldrich and silver nitrate from Loba Chemie. Deionised water was used throughout the entire research work.

2.2 Synthesis of MoO_3 and silver doped MoO_3 nanoparticles

For the synthesis of MoO_3 nanoparticles, 2.43 g of AHM ($[NH_4]_6Mo_7.O_{24}.4H_2O$]) was dissolved in 10 mL of deionised water. After stirring for 15 mins, 10 mL of Con. HNO_3 was added slowly in the aqueous solution containing AHM. The reaction mixture was then transferred to Teflon lined stainless steel autoclave (100 mL) and heated at 90 ^oC for 9 hours. The system was then allowed to cool naturally to room temperature. The obtained precipitate was collected by centrifugation and washed several times with deionised water and ethanol. Finally the powder was dried in vacuum oven at 70 ^oC for 12 hours. Similar procedure was followed for synthesizing Ag doped MoO_3. During the reaction, silver nitrate was added along with AHM. The synthesis was carried out for three different weight percentages (1%, 3% & 5%) of silver nitrate along with AHM. The synthesized nanoparticles MoO_3, 1% Ag doped MoO_3, 3% Ag doped MoO_3 and 5% Ag doped MoO_3 which is mentioned as M, 1AM, 3AM and 5AM respectively. The formation of molybdenum trioxide from the precursor can be described by the following endothermic reaction,

$$(NH_4)_6Mo_7O_{24}4H_2O \longrightarrow 7MoO_3(s) + 6NH_3\,(g) + 7H_2O(g)$$

2.3 Characterization techniques

X-ray diffraction patterns of the synthesized samples were recorded on X'pert PRO powder X-ray diffractometer in 2θ range of 20°–60° at a scan rate of 2° min^{-1} using Cu-Kα X-ray radiation source. The surface morphologies of the samples were examined by using field emission scanning electron microscope ((JSM-6700, JEOL, Japan). The elemental compositions were obtained on Energy Dispersive X-ray spectrometer (RONTEC's EDX system, Model QuanTax 200, Germany). The HRTEM images were obtained using High Resolution Transmission Electron Microscope (JEM-2100 Plus, JEOL, Japan). The FTIR spectra of the samples were recorded on SHIMADZU spectrometer having ATR facility by pelletizing the samples with KBr in the frequency range of 400–4000 cm^{-1}. FT Raman spectra were recorded using 1064 nm line of Nd:YAG laser as excitation wavelength on an EZ Raman, Enwave optronics, and USA IFS 66 V spectrometer. For recording UV–Vis absorption spectra, a computer controlled JASCO V-530 dual beam spectrophotometer coupled with DRS support was used.

2.4 Antimicrobial studies

Antimicrobial activity of the nanoparticles was carried out against four different bacterial strains i.e. *Staphylococcus aureus, Bacillus cereus, Citrobacter koseri and Pseudomonas aeruginosa* employing well diffusion method. It was performed by properly sterilizing the Mueller Hinton media of agar. After solidification, the wells were cut using a cork borer. The bacterial pathogens to be tested were swabbed onto the surface of Mueller Hinton agar plates. The cut pieces of thin film of samples were placed on the well. The plates were incubated at 37ºC for 24 hours, and then the zone of inhibition was measured in millimeters. Each antibacterial assay was performed in triplicate and mean values were reported.

2.5 Seed Germination

The experimental treatments involved four samples M, 1AM, 3AM and 5AM NPs for observing the germination of foxtail millet (*Setaria italica (L.) P.Beauv.*) and finger millet (*Eleusine coracana (L.) Gaertn.)* seeds. Healthy seeds of uniform size were selected to minimize the errors and were rinsed using water to clean them from chemicals and surface impurities. After rinsing the seeds in running tap water, they were incubated in a 5% (v/v) detergent solution for 5 min. Then, seeds were then immersed in 70% (v/v) ethanol solution (1 min) and finally in NaCl (1.5% (v/v), 10 min). Finally, the seeds were washed twice thoroughly in sterile distilled water. The experiment was performed under normal laboratory conditions in natural light. Germination tests were done in petri dishes containing a Whatman No-1 filter paper moistened with 5 ml of suspension or distilled water and each plate was loaded with fifteen seeds with 5ml suspension of NPs with specific concentration. The distilled water was utilized in control sample for the reference. The petri dishes were kept in a dark place and the number of seeds germinated and other relevant parameters were recorded on daily for a period of 7 days.

3. Results and discussion

3.1 X-Ray Diffraction studies

The crystal structure of MoO_3 and Ag doped MoO_3 were analyzed by powder XRD measurements. The presence of sharp diffraction peaks is an indication of the high crystallinity of the synthesized nanoparticles. The peak with maximum intensity was observed at 25.6° and corresponds to the diffraction from (210) plane of MoO_3. All the other observed diffraction lines at 2θ = 19°, 29°, 36° and 45° were corresponds to the (200), (300), (310), and (410) reflection lines of MoO_3, respectively. All the observed diffraction peaks have been indexed and matched well with standard data card (JCPDS-21-0569). It was found

that the diffraction peaks were ascribed to a metastable hexagonal phase of MoO_3 [16]. The absence of any other diffraction peaks indicates the purity of the MoO_3.

X-ray diffraction information reveals the microstructural details and different structural parameters. The lattice constants "a," "b," and "c" for h-MoO_3 can be determined from the inter-planar spacing values of {h, k, l} planes with the Miller indices h, k, l by using the following equation [17]:

$$\frac{1}{d_{hkl}^2} = \frac{4}{3}\left[\frac{h^2 + hk + k^2}{a^2}\right] + \frac{l^2}{c^2}$$

where, d_{hkl} is the inter-planar spacing of the {h, k, l} plane. The calculated values of lattice parameters for preferential orientation were given in table 1. The values are in good agreement with standard results for hexagonal phase and previously reported values [18].

The crystallite size (D) can be determined from Debye–Scherrer's equation [19]:

$$D = \frac{K\lambda}{\beta_{hkl}\cos\theta_{hkl}}$$

where D,is the crystallite size, the wavelength of X-ray radiation, λ = 1.54056 Å for CuK_α, the shape factor and constant (K = 0.90), β_{hkl} is the instrumental corrected full-width at half-maximum height (FWHM) of the diffraction peak (in radians) located at 2θ and θ_{hkl} the Bragg angle (in degrees), respectively. The calculated values of crystallite sizes for the nanoparticles are provided in table 1. From the XRD pattern, it is observed that the crystallite size of MoO_3 was also found to decrease slightly with Ag doping.

Table 1 Calculated lattice parameters and crystallite size for the nanoparticles

NPs	Lattice parameters		Crystallite size (nm)
	a=b (Å)	c(Å)	
M	10.590	14.902	22.81
1AM	10.598	14.902	22.78
3AM	10.599	14.916	21.27
5AM	10.592	14.908	19.31

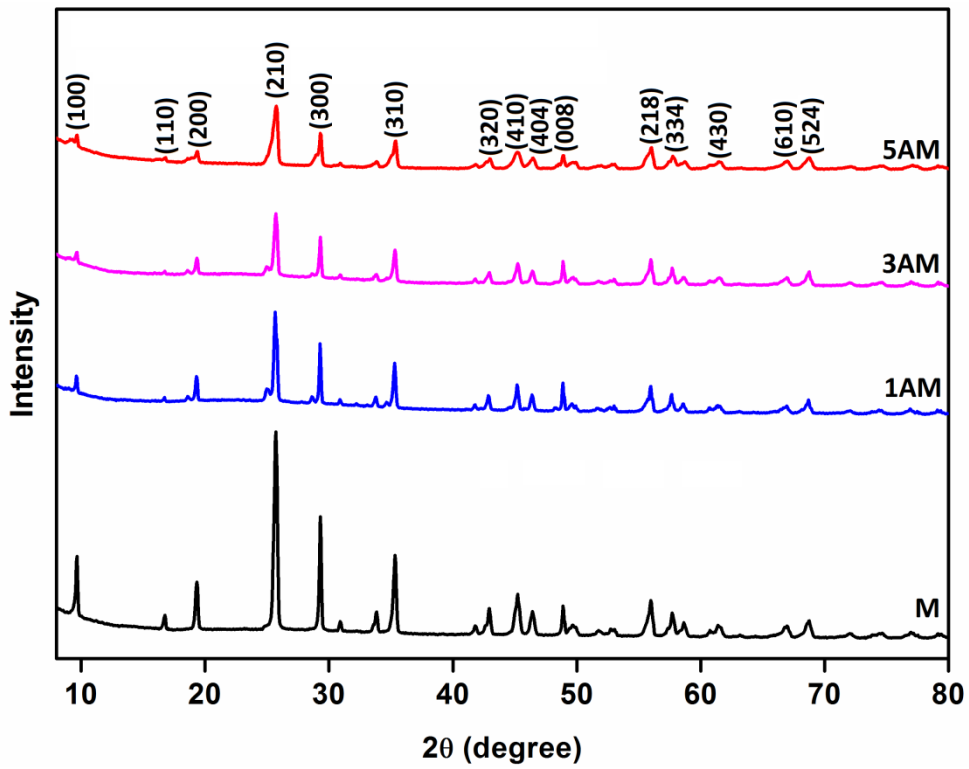

Fig. 1 XRD patterns of MoO_3 and Ag doped MoO_3 nanoparticles

3.2 Morphological studies

The morphology of pure and Ag doped h-MoO_3 NPs were revealed by SEM and the representative images are shown in Fig. 2 (a-h). The shape of MoO_3 crystals is found to be straight hexagonal rods. The projection and side view of the h-MoO_3 sample also shows the uniform growth of the crystals with rod-shaped morphology. It showed that the reaction conditions were perfect for the growth of hexagonal microrods. The rapid nucleation leads to the formation of hexagonal rods and the incorporation of small amount of silver ions in the lattice did not make a considerable impact on their morphology. Fig. 3 (a-d) shows the EDS spectra of MoO_3 and Ag doped h-MoO_3 NPs. The composition of MoO_3 and Ag doped MoO_3 NPs, as determined from energy dispersive X-ray spectroscopy analysis, confirms the presence of molybdenum (in slight excess) along with oxygen and silver. The elements present in the samples confirmed the expected elemental composition. Figure 4 (a-d) shows the HRTEM images of h-MoO_3 (M) and Ag doped h-MoO_3 (5AM) nanoparticles. The fringes

which are observed clearly in the HRTEM image provide the d spacing of the crystal plane from which the X-rays got diffracted. The d spacing of M and 5AM obtained are 0.347 nm and 0.346 nm respectively corresponds to the plane (210).

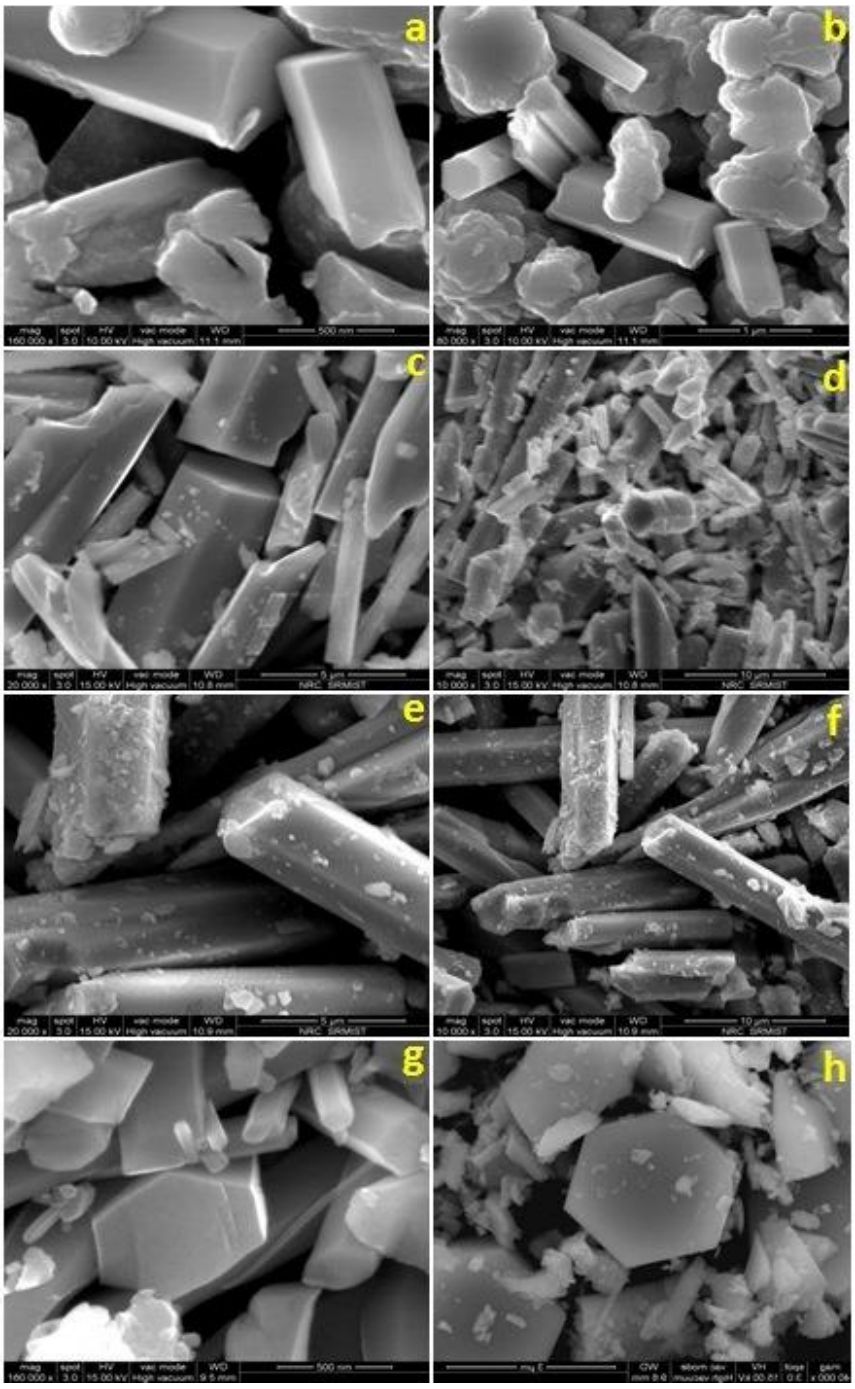

Fig. 2 Representative SEM images of MoO_3 and Ag doped MoO_3 nanoparticles M (a,b), 1AM (c,d), 3AM (e,f) and 5AM (g,h)

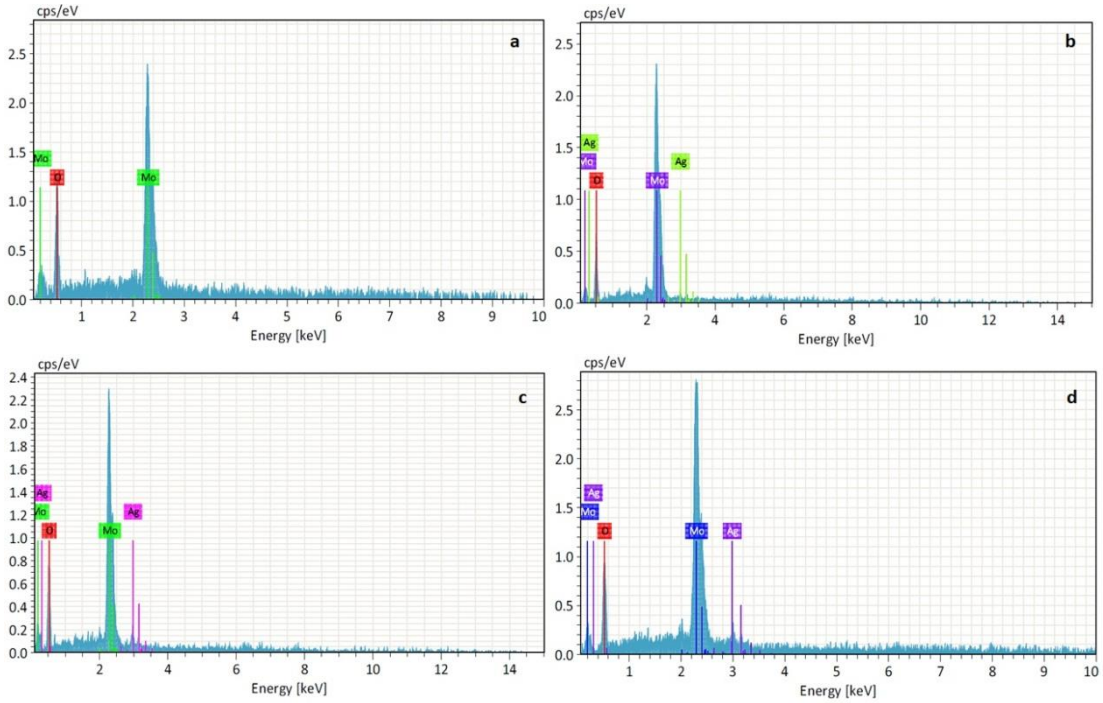

Fig. 3 EDX spectra of MoO_3 and Ag doped MoO_3 nanoparticles (a) M, (b) 1AM, (c) 3AM and (d) 5AM

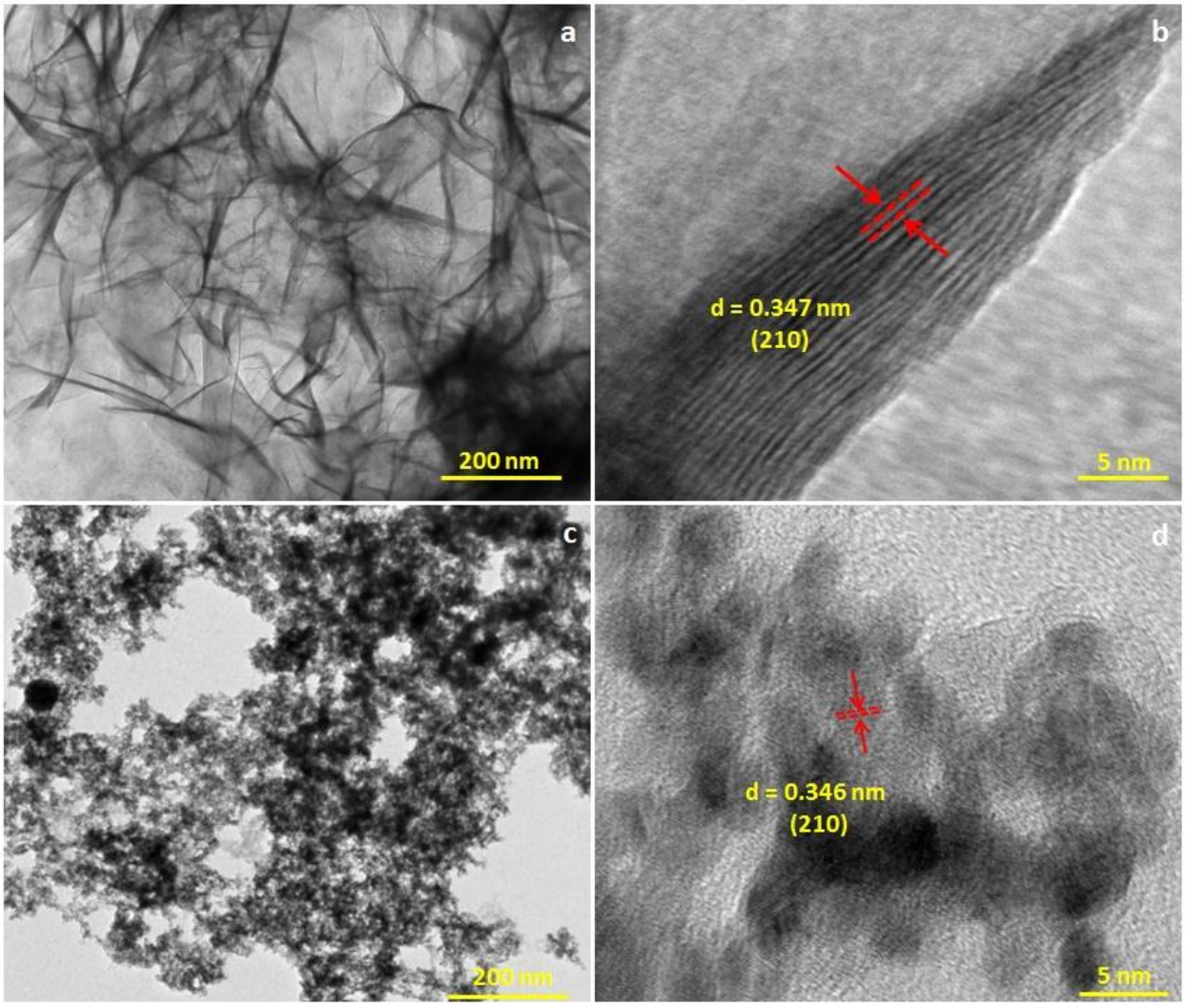

Fig. 4 HRTEM images of (a,b) h-MoO_3, and (c,d) 5% Ag doped MoO_3 nanoparticles

3.3 FTIR spectral studies

The functional groups of the products with the best crystalline degree were identified by FTIR (Fig. 5) over the range of 4000–400 cm^{-1}. For MoO_3 and Ag doped MoO_3 NPs, the peaks obtained in the range of 3437 cm^{-1} and 1636 cm^{-1} correspond to the stretching as well as bending vibrations of O–H bonds from adsorbed water molecules [20], respectively. The bands in the range 2924 cm^{-1} and 1445 cm^{-1} can be ascribed to the stretching and bending vibrations of N–H of NH_4^+ groups which are well consistent with the previous report in literature [21]. The peaks at 974 cm^{-1} and 919 cm^{-1} are ascribed to the oxygen symmetry stretching mode of Mo=O [22]. The bands in the range 574 cm^{-1} is due to the stretching and bending vibrational modes of O-Mo-O bonds with varying Mo-O bond lengths [23]. The above mentioned vibrational bands are the typical characteristics of *h*-MoO_3 phase amidst other phases of MoO_3.

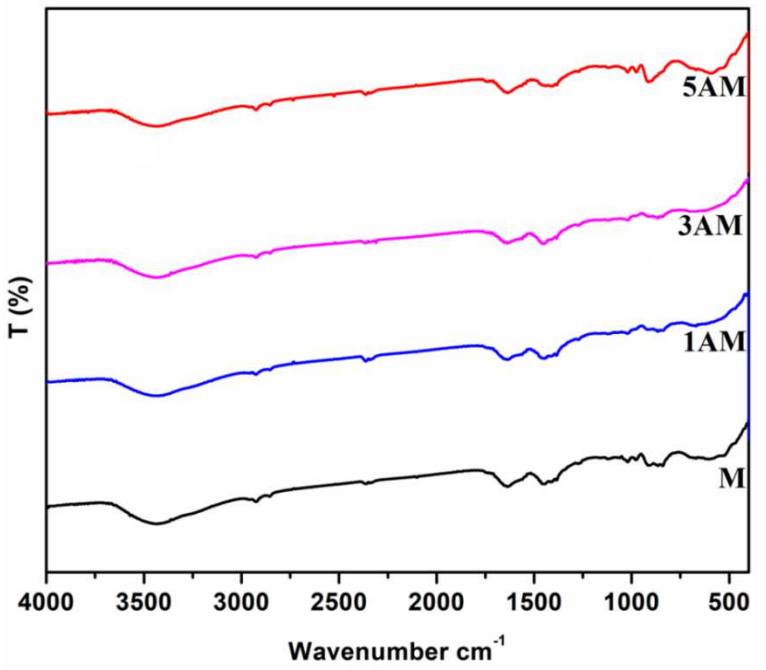

Fig. 5 FTIR spectra of MoO_3 and Ag doped MoO_3 nanoparticles

3.4 Raman spectral studies

The Raman spectra of MoO_3 and Ag doped MoO_3 NPs in the frequency range of 100–1100 cm^{-1} at ambient condition is shown in Fig 6. The sharp band at 987 corresponds to the

terminal oxygen asymmetric stretching of Mo=O and two bands at 906 cm^{-1} & 888 cm^{-1} corresponds to the symmetric stretching mode of (Mo=O) respectively [24]. The sharp band appeared at 688 cm^{-1} corresponds to scissoring vibration of O-Mo-O. The band between 483 to 385 cm^{-1} attributes to the rocking and scissoring modes of triply coordinated oxygen O-Mo-O. The bands appeared between 200 and 300 cm^{-1} originate from the twisting vibrations of MoO_6 octahedra [25]. The Raman bands observed below 200 cm^{-1} corresponds to the deformation and lattice modes [26]. The observed vibrational peak positions confirm the formation of h-MoO_3 with phase purity. Upon doping, no such Raman bands related to Ag were observed which confirms successful incorporation of Ag^+ ions into the lattice sites of h-MoO_3.

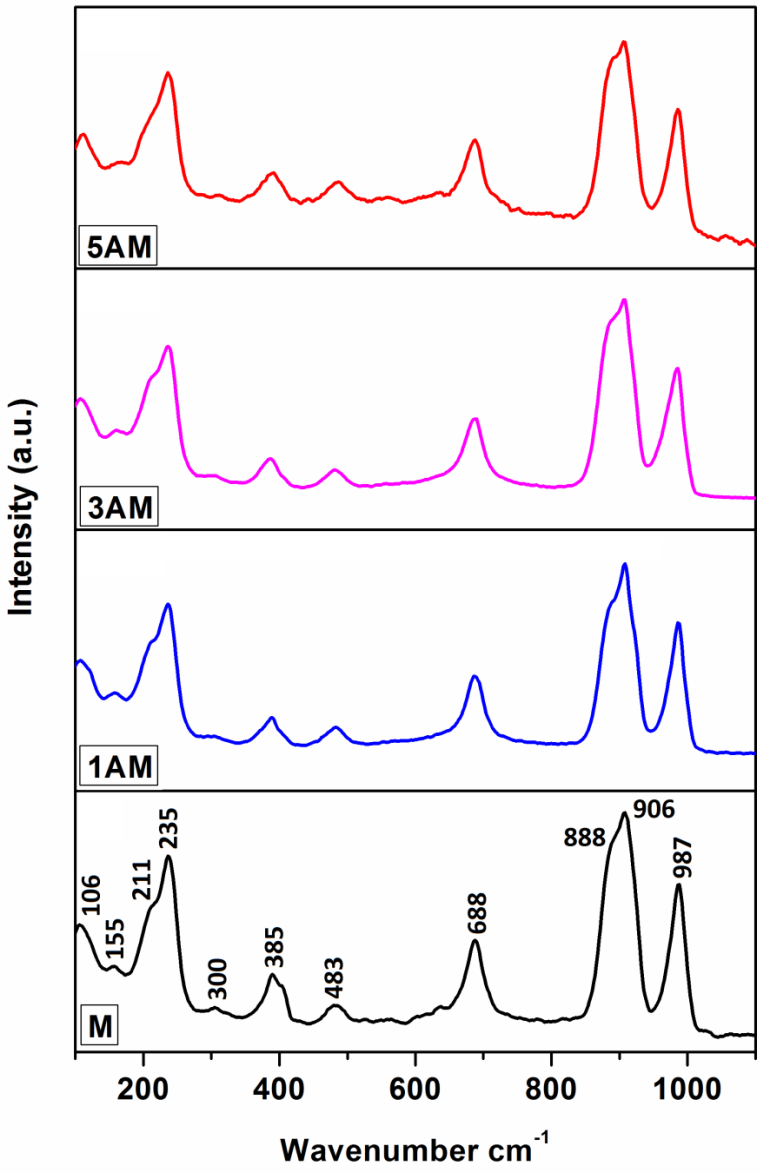

Fig. 6 Raman spectra of MoO_3 and Ag doped MoO_3 nanoparticles

3.5 UV-DRS spectra

The optical behaviour of MoO_3 and Ag doped MoO_3 nanoparticles were studied using UV-visible absorbance spectra (Fig. 7a) recorded in the wavelength range of 200-800 nm. The sharp absorption edge around 418 nm corresponding to h-MoO_3 indicates that the visible light absorption can be attributed to the electronic band gap transition [27]. The indirect band gap energies of the synthesised nanoparticles were obtained from the Plot of F(R) vs photon energy (hν) derived from the Kubelka-Munk function [28]:

$$F(R) = \frac{(1-R)^2}{2R} = \frac{K(\lambda)}{S(\lambda)} \infty \alpha = \frac{(h\upsilon - E_g)^n}{h\upsilon}$$

Where, R denotes the diffuse reflectance of the samples, where F(R) is the K–M function, K(λ) is the absorption coefficient, S(λ) is the scattering coefficient, hυ is the photon energy, n=1/2 (indirect band gap) and E_g is the band gap energy for indirect transition, respectively. The optical indirect band gap can be determined from tangent drawn at the curve obtained by plotting of $(F(R)h\upsilon)^{1/2}$ vs photon energy (hυ) (Fig. 7b). The band gap energies of the nanoparticles M, 1AM, 3AM & 5AM were found to be 3.26 eV, 3.22 eV, 2.94 eV and 2.76 eV respectively. This trend shows the decrease in band gap energy with increasing the dopant concentrations.

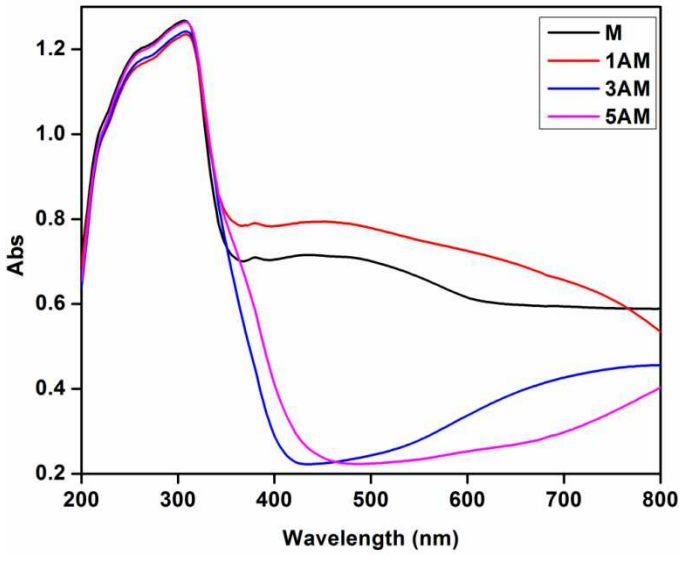

Fig. 7a Absorbance spectra of MoO_3 and Ag doped MoO_3 nanoparticles

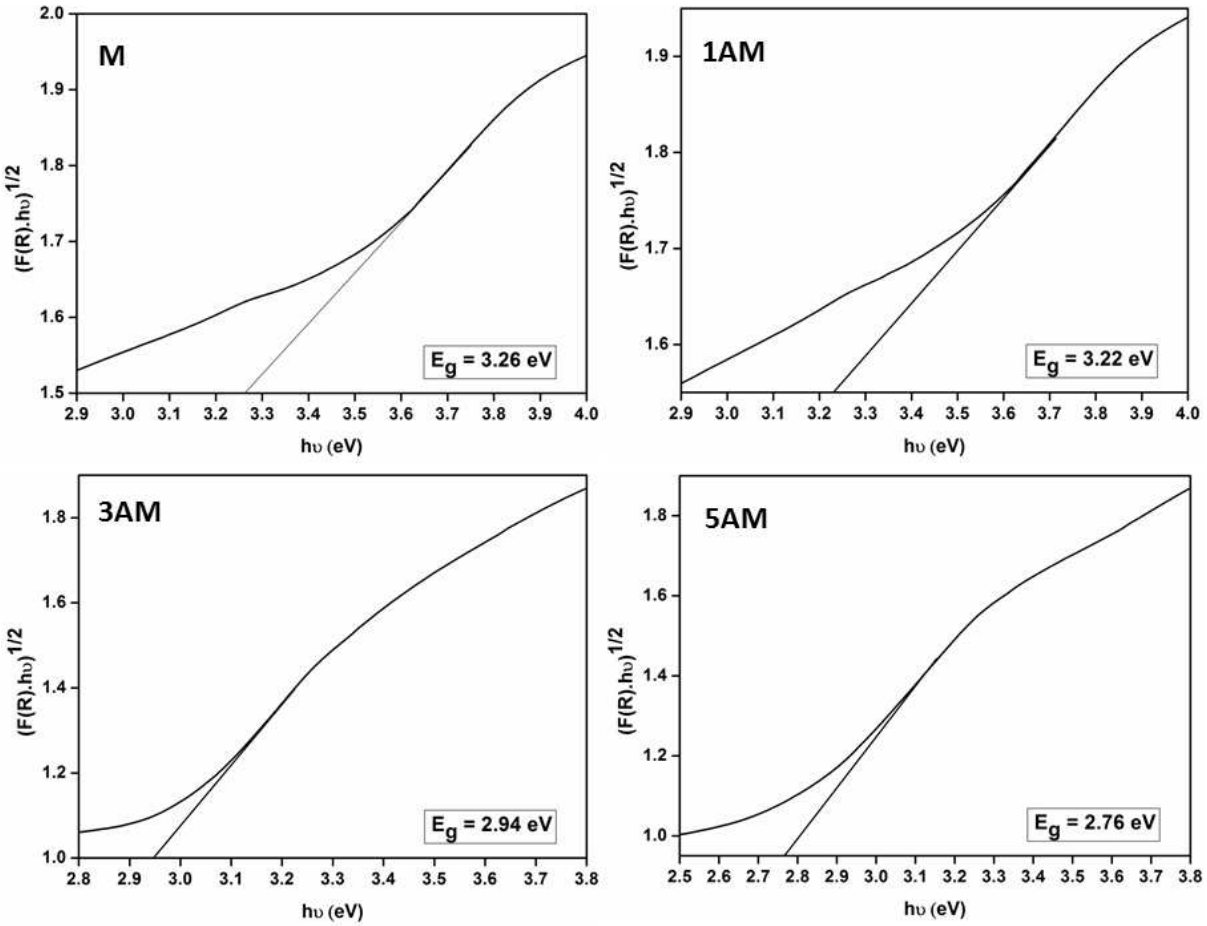

Fig. 7b Band gap calculation using Kubelka–Munk (K–M) function for MoO_3 and Ag doped h-MoO_3 nanoparticles

3.6 Antimicrobial studies

Antibacterial properties of h-MoO_3 and Ag doped h-MoO_3 are explored against two gram positive and two gram negative bacterial strains via well diffusion method. Antibacterial activity was performed for 100 μg/mL dosage of the nanoparticles (Fig. 8a).

It is observed that the biocidal effect of h-MoO_3 improves with increasing the concentration of Ag against *Staphylococcus aureus, Citrobacter koseri and Pseudomonas aeruginosa.* For *Staphylococcus aureus*, no significant activity is observed for h-MoO_3 NPs. But for the gram positive bacteria (*Bacillus cereus),* the zone of inhibition is found to be

decreased from 12 mm to 07 mm for an increasing amount of dopant (Ag) concentration in h-MoO_3 nanoparticles. The highest zone of inhibition was observed against *Pseudomonas aeruginosa* for 5AM and it is found to be 23 mm in diameter.

To explain the mechanism, it is necessary to understand the interaction between nanoparticle and bacterial cell wall which leads to the destruction of the cell wall [29]. Along with this, the size, shape, structure and composition of nanomaterials also play a crucial role in the bactericidal effect [30].

Silver present in the form of Ag^+ is more easily released and directly react with cell membranes when immersed in a practical biological system. But the Ag metal bound to the h-MoO_3 particles must first undergo dissolution to form Ag^+ and then migrate into the bacterial cell [31]. It is known that, silver ions could easily interact with a number of electron donor groups like phosphates, thiols, hydroxyls, indoles and imidazoles thereby causing damage to the cell membrane and releasing the ROS, finally causing bacterial death [32].

It can be assumed that with decreasing particle size, the number of particles per unit volume increases resulting in increased surface area and increased generation of hydrogen peroxide [33]. The hydrogen peroxide, hydroxyl radicals, and superoxide allied to ROS group can harm the DNA and may cause the cell death. The histogram (Fig. 8b) and the values provided in table 2 shows the bacterial growth inhibition zone in the presence of h-MoO_3 and Ag doped h-MoO_3 NPs.

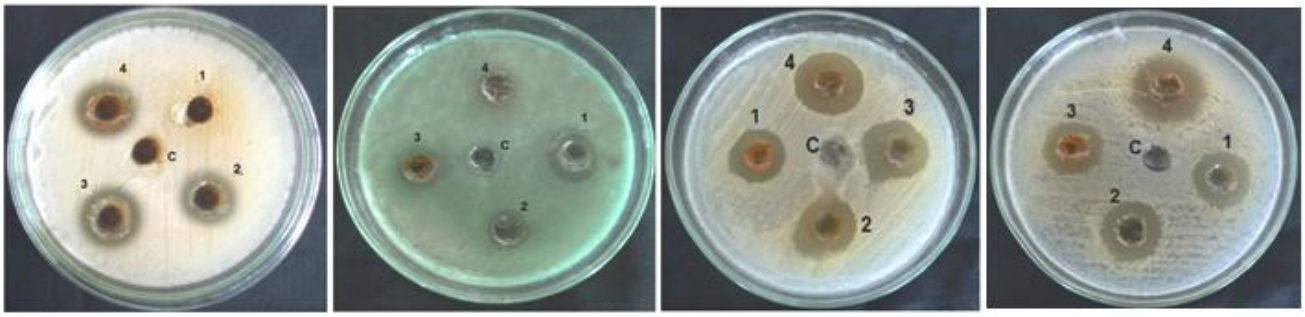

Fig 8a. Antimicrobial properties of NPs against various bacterial strains

Table 2 Antibacterial effects of NPs against various bacterial strain

NPs	Representation of zone of inhibition (diameter in mm)			
	Antibacterial activity (100 µg/mL)			
	Staphylococcus aureus	***Bacillus cereus***	***Citrobacter koseri***	***Pseudomonas aeruginosa***
M	-	12±0.4	16±0.7	17±0.3
1AM	13±0.4	09±0.2	18±0.4	19±0.1
3AM	15±0.3	10±0.4	20±0.1	19±0.5
5AM	15±0.7	07±0.9	22±0.5	23±0.4

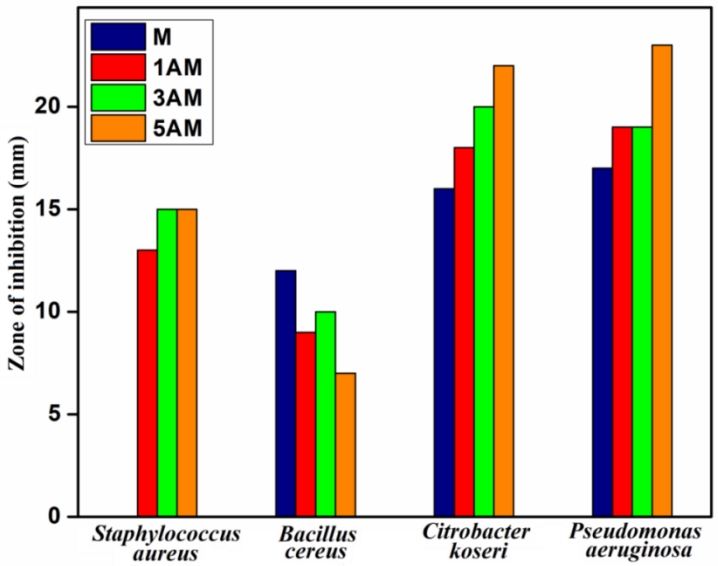

Fig 8b. Zone of inhibition for bacterial growth by h-MoO_3 and Ag doped h-MoO_3 nanoparticles

3.7. Seed Germination of Foxtail millet and finger millet seeds

The prepared h-MoO_3 and Ag doped h-MoO_3 NPs are used as fertilizer for improving the growth of foxtail and finger millet seeds at room temperature. Both the seeds were germinated for seven days and then various parameters were recorded such as root and shoot length, seed vigor index and germination percentage are presented in figure 10.

The germination percentage and the seed vigor index are the indicators for the enhancement in germination rate of the seeds. The growth response of seeds in the presence of h-MoO_3, Ag doped h-MoO_3 and distilled water are analysed.

The germination percentage and the quality of germinated seeds can be identified by calculating the seed vigor index using the following equation [34].

$$[Germination\ \%\ ] = \frac{No.of\ germinated\ seeds}{No.of\ inoculated\ seeds}\ \text{X}\ 100$$

$$Seed\ vigor\ index = [Germination\ \%]\ \text{X}\ [Mean\ shoot\ length + Mean\ root\ length]$$

It is clear from the results that there is enhancement in germination rate of the foxtail millet (Table 3 & Fig. 9a) and finger millet seeds (Table 4 & Fig. 9b) after treating with the NPs. The germination percentage and the seed vigor indices were increased for M, 1AM and 3AM samples in both type of seeds but decreased slightly for 5AM sample, indicating that the moderate nanoparticle concentration is effective for seed growth.

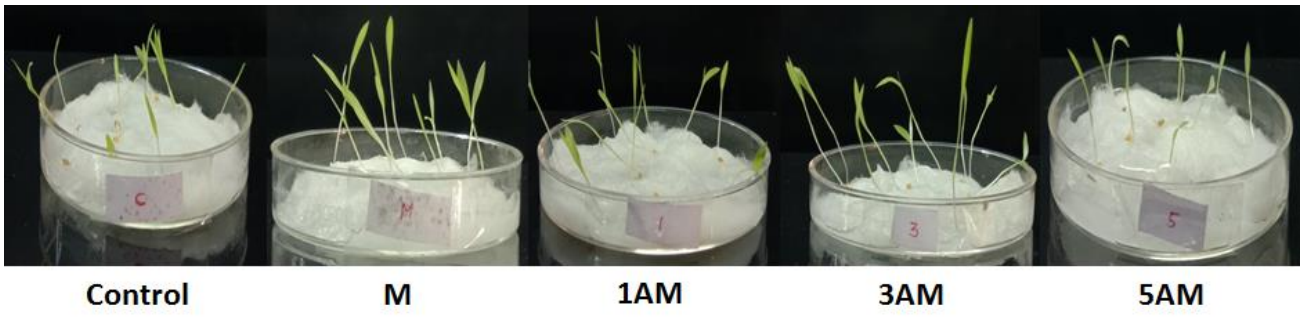

Fig 9a. Germination of Foxtail millet seeds by MoO_3 and Ag doped MoO_3 nanoparticles

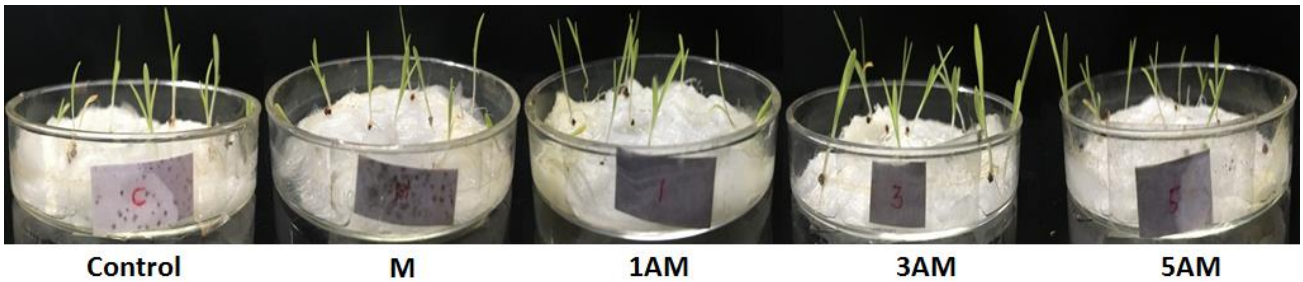

Fig 9b. Germination of Finger millet seeds by MoO_3 and Ag doped MoO_3 nanoparticles

Therefore, it is evident that the uptake of h-MoO_3 and Ag doped h-MoO_3 NPs (1-5%) by both the seeds, increased their percentage germination but the germination being

prohibited for higher Ag concentration (5%) due to toxicity and the results are in consistent with literature [35].

Table 3 Mean performance of Foxtail millet seeds germination

Sample name	Germination percentage (%)	Seed vigor index	Root length (cm)	Shoot length (cm)
Control	53	208.82	0.97	2.97
M	66	343.86	1.35	3.86
1AM	73	399.31	1.37	4.1
3AM	86	608.88	1.8	5.28
5AM	60	207.60	0.74	2.72

Table 4 Mean performance of Finger millet seeds germination

Sample name	Germination percentage (%)	Seed vigor index	Root length (cm)	Shoot length (cm)
Control	40	162	1.21	2.84
M	53	248.04	1.50	3.18
1AM	60	343.80	1.77	3.96
3AM	73	456.25	1.98	4.27
5AM	33	132	1.33	2.69

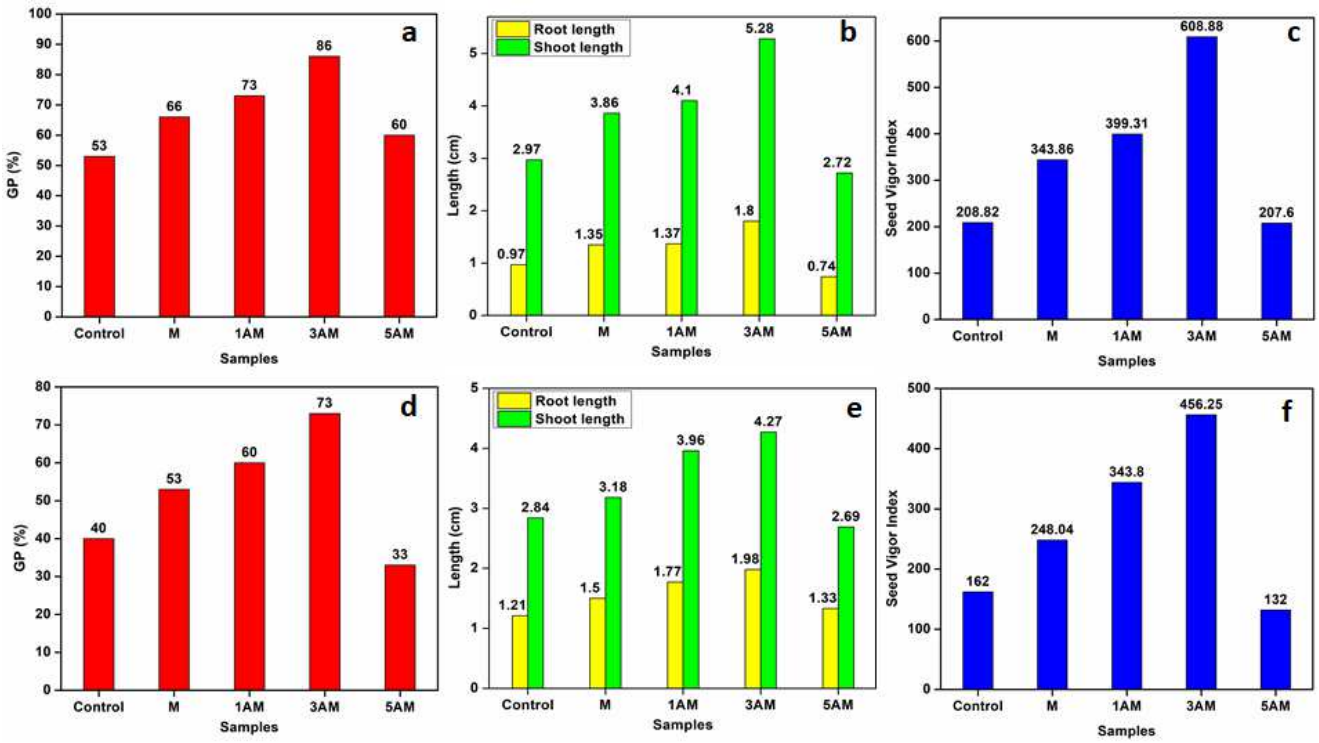

Fig 10. (a,d) Germination percentage, (b,e) Root and shoot length, and (c,f) seed vigour index of foxtail millet and finger millet seeds respectively treated with MoO_3 and Ag doped MoO_3 nanoparticles

Many researchers have reported the impact produced by nanoparticles on seeds germination, but, the exact mechanism is still not well-understood. It is generally observed that the h-MoO_3 and Ag doped h-MoO_3 NPs can penetrate into the seed coat and activate the embryo so as to increase the uptake of water and other nutrients [36]. During the penetration of the h-MoO_3 NPs more new pores are created which absorb the nutrients and thereby increasing the seed germination percentage and growth rate.

The enhanced growth rate of seeds may be due to uptake of water (for supplying energy to the seeds which is essential for germination) and nutrients by the treatment with nanoparticles [37]. The increase in the seed growth might be due to molybdenum, an important micronutrient for plant growth which is involved in several oxidation-reduction processes in plants. Accordingly, the NPs are proved to have positive effects in promotion of

root and shoot formation, and also accumulation of plant biomass from seeds in most of the crops compared to the untreated one [38].

Silver based nanoparticles are commonly used in the food and agriculture application at specified concentrations due to their well-known antimicrobial activity and root regeneration property. The highest concentration tested for Ag doped NPs (higher concentrations induce oxidative stress in plant cells) was not found to be effective for plant growth but had a robust antimicrobial effect, which would be beneficial in during seed germination period. The silver doped NPs at moderate concentrations significantly enhance seed germination, germination %, seed vigour index, root length and shoot length of seeds. Even higher concentrations of Ag doped NPs have led to a severe decrease in the growth parameters of seeds which were associated with accumulation of Ag in the stems and roots [39].

4. Conclusion

The h-MoO_3 and different concentrations of Ag doped h-MoO_3 NPs were successfully synthesized by autoclave mediated hydrothermal route. Powder XRD analysis shows that the Ag doped MoO_3 NPs crystallize in meta-stable hexagonal structure with (210) preferred orientation. Further the FTIR, Raman and SEM-EDX studies confirms the formation of phase pure h-MoO_3 and Ag doped h-MoO_3 NPs. The morphology of the synthesized h-MoO_3 and Ag doped h-MoO_3 shows the rod like structure with hexagonal cross section. From HRTEM analysis, the crystallite size was found to decrease slightly for the Ag doped h-MoO_3 compared to pure h-MoO_3 NPs. From the UV-DRS spectra, the indirect band gap energy was found to decrease from 3.26 eV to 2.76 eV as the concentration of Ag increases and the

reason may be due to the Ag doping can cause great deviations in the electronic structure of the host material. The synthesized h-MoO_3 and Ag doped h-MoO_3 NPs exhibit good inhibitory action against four bacterial strains *viz. Staphylococcus aureus, Bacillus cereus, Citrobacter koseri and Pseudomonas aeruginosa.* The h-MoO_3 and Ag doped h-MoO_3 NPs displayed tremendous germination growth of foxtail and finger millet seeds upto 86% and 73%, respectively, and therefore can be employed as a promising fertilizer in the plant growth. Because of the toxicity, 5% Ag doped h-MoO_3 NPs study had little negative effect on seedling growth for both the seeds, but shows the maximum zone of inhibition against all the bacterial strains.

Declarations

The authors declare no conflict of interest.

Acknowledgments

The authors thank the management of St. John's College, Tirunelveli, Tamil Nadu also being our research centre for providing the lab facilities to carry out this research work. We would like to acknowledge SRM University, Chennai, Tamil Nadu, India for providing PXRD and SEM with EDX spectral analysis. We thank Dr.C. Vethi, VOC College, Tuticorin, for recording FTIR and UV-DRS spectra. Also we would like to thank the Department of Nanotechnology, Noorul Islam centre for higher Education, Thuckalay, Kanniyakumari, Tamil Nadu-629180, India for recording Raman spectra.

References

[1] R. Prasad, A. Bhattacharyya, Q.D. Nguyen, Nanotechnology in sustainable agriculture: recent developments, challenges, and perspectives, *Front. Microbiol. 8* (2017) 1014.

[2] D. Mittal, G. Kaur, P. Singh, K. Yadav, S.A. Ali, Nanoparticle-based sustainable agriculture and food science: recent advances and future outlook*, Front. Nanotechnol. 2* (2020).

[3] I. Iavicoli, V. Leso, D.H. Beezhold, A.A. Shvedova, Nanotechnology in agriculture: Opportunities, toxicological implications, and occupational risks, *Toxicol. Appl. Pharmacol. 329* (2017) 96-111.

[4] R. Liu, R. Lal, Potentials of engineered nanoparticles as fertilizers for increasing agronomic productions, *Sci. Total Environ. 514* (2015) 131-139.

[5] M. Usman, M. Farooq, A. Wakeel, A. Nawaz, S.A. Cheema, H. ur Rehman, M. Sanaullah, Nanotechnology in agriculture: Current status, challenges and future opportunities, *Sci. Total Environ. 721* (2020) 137778.

[6] A. Manivel, G.J. Lee, C.Y. Chen, J.H. Chen, S.H. Ma, T.L. Horng, J.J. Wu, Synthesis of MoO_3 nanoparticles for azo dye degradation by catalytic ozonation, *Mater. Res. Bull. 62* (2015)184-191.

[7] C.V. Ramana, I.B. Troitskaia, V.V. Atuchin, M. Ramos, D. Ferrer, Electron microscopy characterization of hexagonal molybdenum trioxide (MoO_3) nanorods, *J. Vac. Sci. Technol. A 28* (2010) 726-729.

[8] J. Song, X. Ni, L. Gao, H. Zheng, Synthesis of metastable h-MoO_3 by simple chemical precipitation, *Mater. Chem. Phys. 102* (2007) 245-248.

[9] L. Zhou, L. Yang, P. Yuan, J. Zou, Y. Wu, C. Yu, α-MoO_3 nanobelts: a high performance cathode material for lithium ion batteries, *J. Phys. Chem.* ***C*** *114* (2010) 21868-21872.

[10] C. Chaves-Lopez, H.N. Nguyen, R.C. Oliveira, E.T. Nadres, A. Paparella, D.F. Rodrigues, A morphological, enzymatic and metabolic approach to elucidate apoptotic-like cell death in fungi exposed to h-and α-molybdenum trioxide nanoparticles, *Nanoscale*, *10* (2018) 20702-20716.

[11] C. Zollfrank, K. Gutbrod, P. Wechsler, J.P. Guggenbichler, Antimicrobial activity of transition metal acid MoO_3 prevents microbial growth on material surfaces, *Mater. Sci. Eng.* ***C*** *32* (2012) 47-54.

[12] M. Imran, X. Sun, S. Hussain, U. Ali, M.S. Rana, F. Rasul, C.X. Hu, Molybdenum-induced effects on nitrogen metabolism enzymes and elemental profile of winter wheat (Triticum aestivum L.) under different nitrogen sources, *Int. **J**. Mol. Sci. 20* (2019) 3009.

[13] M.R. Bindhu, M. Umadevi, G.A. Esmail, N.A. Al-Dhabi, M.V. Arasu, Green synthesis and characterization of silver nanoparticles from Moringa oleifera flower and assessment of antimicrobial and sensing properties, *J. Photochem. Photobiol. B* 205 (2020) 111836.

[14] I.X. Yin, J. Zhang, I.S. Zhao, M.L. Mei, Q. Li, C.H. Chu, The antibacterial mechanism of silver nanoparticles and its application in dentistry, *Int. J. Nanomedicine 15* (2020) 2555-2562.

[15] M.S. Sadak, Impact of silver nanoparticles on plant growth, some biochemical aspects, and yield of fenugreek plant (Trigonella foenum-graecum), *Bull. Natl. Res. Cent. 43* (2019) 1-6.

[16] A. Chithambararaj, A.C. Bose, Investigation on structural, thermal, optical and sensing properties of meta-stable hexagonal MoO_3 nanocrystals of one dimensional structure, *Beilstein J. Nanotechnol. 2* (2011) 585-592.

[17] K.V. Alex, A.R. Jayakrishnan, A.S. Ibrahim, K. Kamakshi, J.P.B. Silva, K.C. Sekhar, M.J.M. Gomes, Substrate temperature induced effect on microstructure, optical and photocatalytic activity of ultrasonic spray pyrolysis deposited MoO_3 thin films, *Mater. Res. Express* 6 (2019) 066421.

[18] A. Chithambararaj, N.S. Sanjini, S. Velmathi, A.C. Bose, Preparation of h-MoO_3 and α-MoO_3 nanocrystals: comparative study on photocatalytic degradation of methylene blue under visible light irradiation, *Phys. Chem. Chem. Phys. 15* (2013) 14761-14769.

[19] S.K. Sen, S. Dutta, M.R. Khan, M.S. Manir, S. Dutta, A. Al Mortuza, M.A. Hakim, Characterization and Antibacterial Activity Study of Hydrothermally Synthesized h-MoO_3 Nanorods and α-MoO_3 Nanoplates, *BioNanoScience 9* (2019) 873-882.

[20] K. Nakamoto, Infrared Spectra of Inorganic and Coordination Compounds, John Wiley and Son. *Inc. New york, London* 1963.

[21] L. Fang, Y. Shu, A. Wang, T. Zhang, Template-free synthesis of molybdenum oxide-based hierarchical microstructures at low temperatures*, J. Cryst. Growth 310* (2008) 4593-4600.

[22] K. Kurleto, F. Tielens, J. Handzlik, Isolated Molybdenum (VI) and Tungsten (VI) Oxide Species on Partly Dehydroxylated Silica: A Computational Perspective*, J. Phys. Chem. C 124* (2020) 3002-3013.

[23] P. Thangasamy, V. Shanmugapriya, M. Sathish, One-dimensional growth of hexagonal rods of metastable h-MoO_3 using one-pot, rapid and environmentally benign supercritical fluid processing*, Physica E Low Dimens. Syst. Nanostruct. 99* (2018) 189-193.

[24] J.V. Silveira, J.A. Batista, G.D. Saraiva, J. Mendes Filho, A.G. Souza Filho, S. Hu, X. Wang, Temperature dependent behavior of single walled MoO_3 nanotubes: A Raman spectroscopy study*, Vib. Spectrosc. 54* (2010) 179-183.

[25] J.V.B. Moura, J.V. Silveira, J.G. da Silva Filho, A.G. Souza Filho, C. Luz-Lima, P.T.C. Freire, Temperature-induced phase transition in h-MoO_3: Stability loss mechanism uncovered by Raman spectroscopy and DFT calculations*, Vib. Spectrosc. 98* (2018) 98-104.

[26] C.C. Zhang, L. Zheng, Z.M. Zhang, R.C. Dai, Z.P. Wang, J.W. Zhang, Z.J. Ding, Raman studies of hexagonal MoO_3 at high pressure*, Phys. Status Solidi B 248* (2011)1119-1122.

[27] A. Chithambararaj, N.S. Sanjini, A.C. Bose, S. Velmathi, Flower-like hierarchical h-MoO_3: new findings of efficient visible light driven nano photocatalyst for methylene blue degradation*, Catal. Sci. Technol. 3* (2013) 1405-1414.

[28] M. Paul, M. Dhanasekar, S.V. Bhat, Silver doped h-MoO_3 nanorods for sonophotocatalytic degradation of organic pollutants in ambient sunlight*, Appl. Surf. Sci. 418* (2017) 113-118.

[29] K.S. Siddiqi, A. Rahman, H.A. Tajuddin, Azamal Husen, Properties of zinc oxide nanoparticles and their activity against microbes, *Nanoscale Res. Lett*, *13* (2018) 1-13.

[30] H. Li, Q. Cui, B. Feng, J. Wang, X. Lu, J. Weng, Antibacterial activity of TiO_2 nanotubes: influence of crystal phase, morphology and Ag deposition, *Appl. Surf. Sci. 284* (2013) 179-183.

[31] Z.M. Xiu, Q.B. Zhang, H.L. Puppala, V.L. Colvin, P.J. Alvarez, Negligible particle-specific antibacterial activity of silver nanoparticles, *Nano Lett. 12* (2012) 4271-4275.

[32] A.U. Mirza, A. Kareem, S.A. Nami, M.S. Khan, S. Rehman, S.A. Bhat, N. Nishat, Biogenic synthesis of iron oxide nanoparticles using Agrewia optiva and Prunus persica phyto species: characterization, antibacterial and antioxidant activity, *J. Photochem. Photobiol. B* 185 (2018) 262-274.

[33] N. Sharma, J. Kumar, S. Thakur, S. Sharma, V. Shrivastava, Antibacterial study of silver doped zinc oxide nanoparticles against Staphylococcus aureus and Bacillus subtilis, *Drug Invent. Today 5* (2013) 50-54.

[34] M. Rafique, J. Jahangir, B.A.Z. Amin, M.B. Tahir, G. Nabi, M.I. Khan, I. Sadaf, Investigation of photocatalytic and seed germination effects of TiO_2 nanoparticles synthesized by Melia azedarach L. Leaf extract, *J Inorg Organomet Polym Mater. 2* (2019) 2133-2144.

[35] A. Elizabath, V. Bahadur, P. Misra, V.M. Prasad, T. Thomas, Effect of different concentrations of iron oxide and zinc oxide nanoparticles on growth and yield of carrot (Daucus carota L.), *J. Pharmacogn. Phytochem. 6* (2017) 1266-1269.

[36] M.I. Khan, N. Fatima, M. Shakil, M.B. Tahir, K.N. Riaz, M. Rafique, K. Mahmood, Investigation of in-vitro antibacterial and seed germination properties of green synthesized pure and nickel doped ZnO nanoparticles, *Physica B Condens. 601* (2021) 412563.

[37] N. Savithramma, S. Ankanna, G. Bhumi, Effect of nanoparticles on seed germination and seedling growth of Boswellia ovalifoliolata an endemic and endangered medicinal tree taxon*, Nano Vision*, *2* (2012) 61-68.

[38] S.A. Osman, D.M. Salama, M.E. Abd El-Aziz, E.A. Shaaban, M.S. Abd Elwahed, The influence of MoO_3-NPs on agro-morphological criteria, genomic stability of DNA, biochemical assay, and production of common dry bean (Phaseolus vulgaris L.), *Plant Physiol. Biochem. 151* (2020) 77-87.

[39] R. Prażak, A. Święciło, A. Krzepiłko, S. Michałek, M. Arczewska, Impact of Ag Nanoparticles on Seed Germination and Seedling Growth of Green Beans in Normal and Chill Temperatures*, Agriculture*, *10* (2020) 312.

Figures

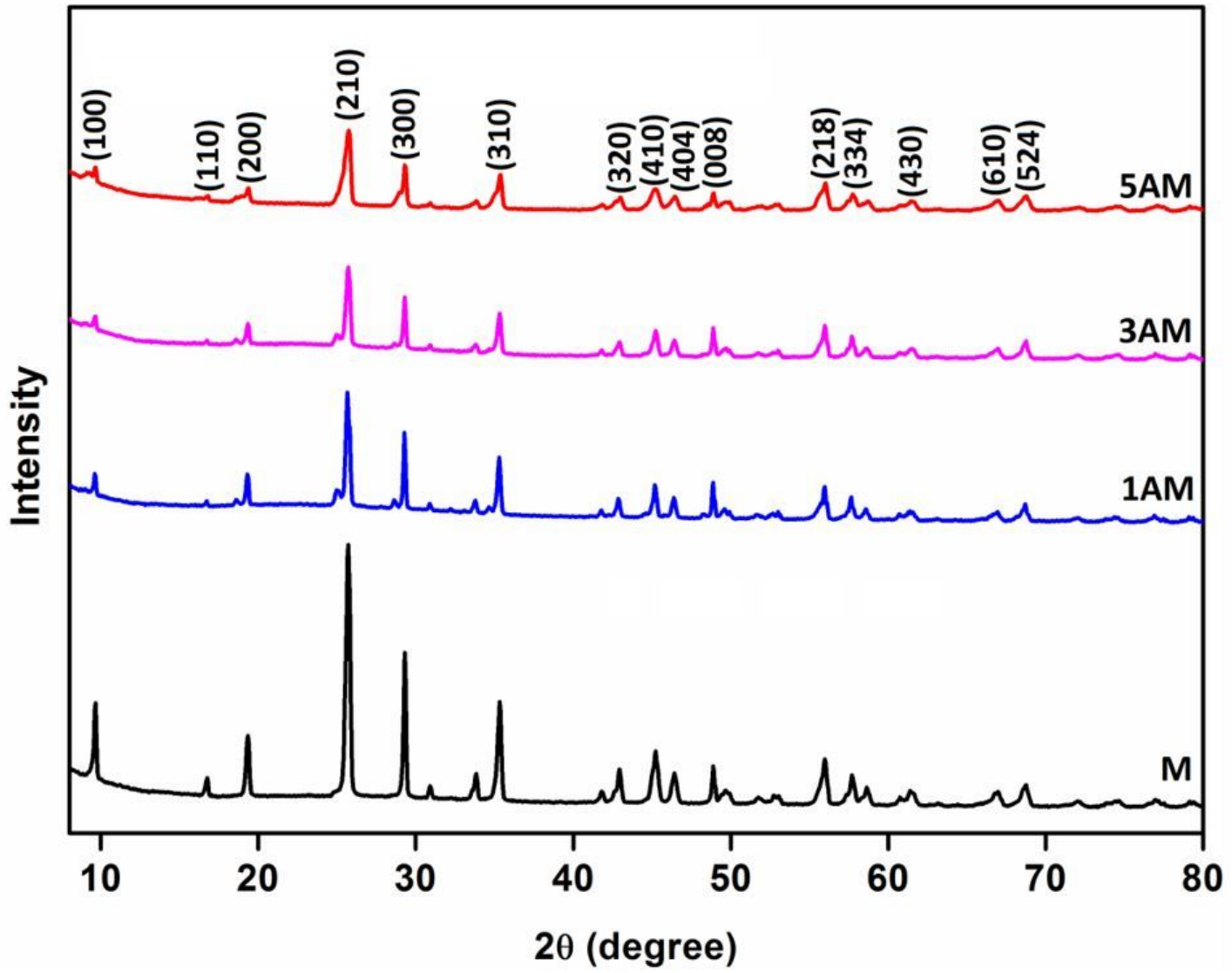

Figure 1

XRD patterns of MoO3 and Ag doped MoO3 nanoparticles

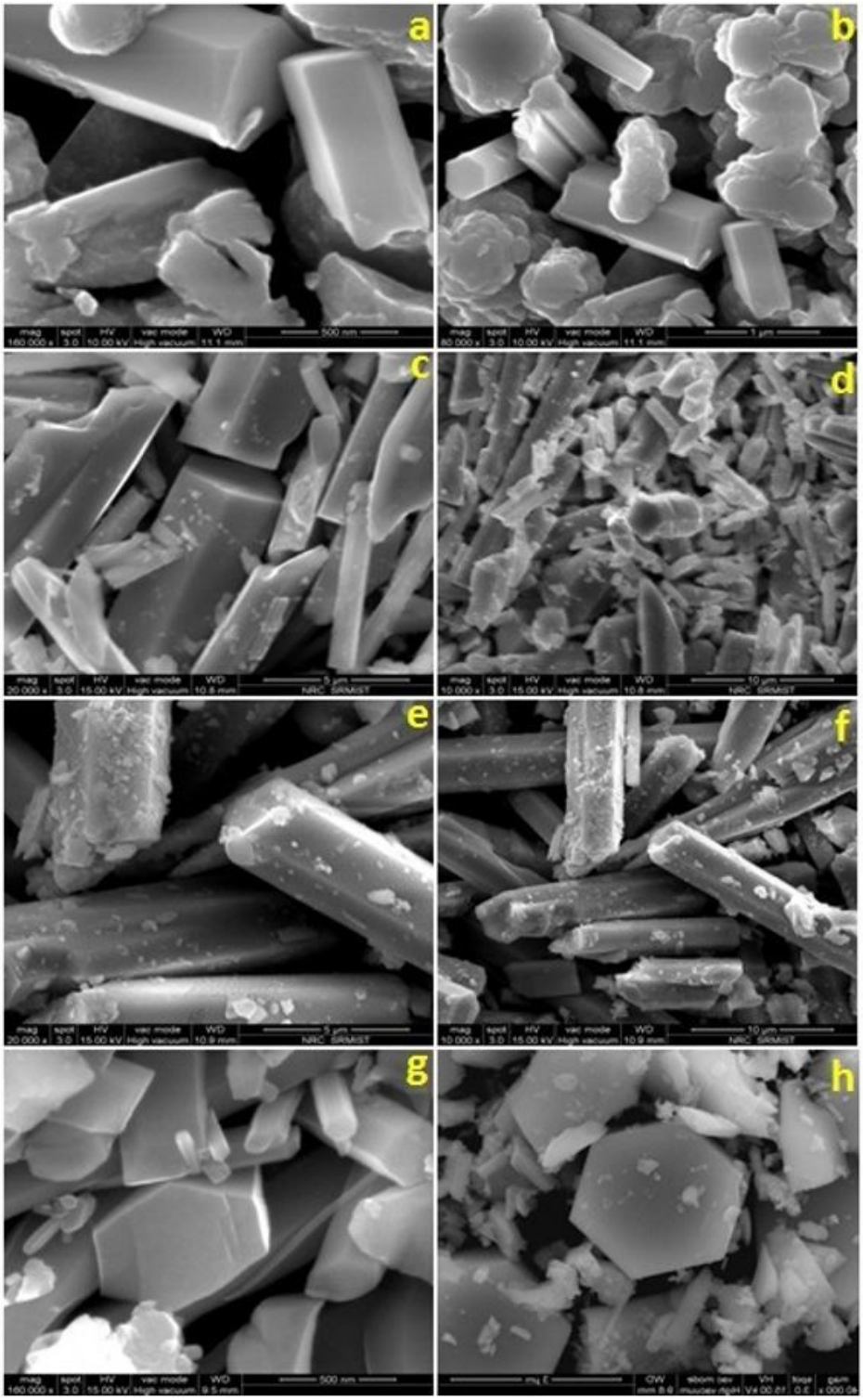

Figure 2

Representative SEM images of MoO3 and Ag doped MoO3 nanoparticles M (a,b), 1AM (c,d), 3AM (e,f) and 5AM (g,h)

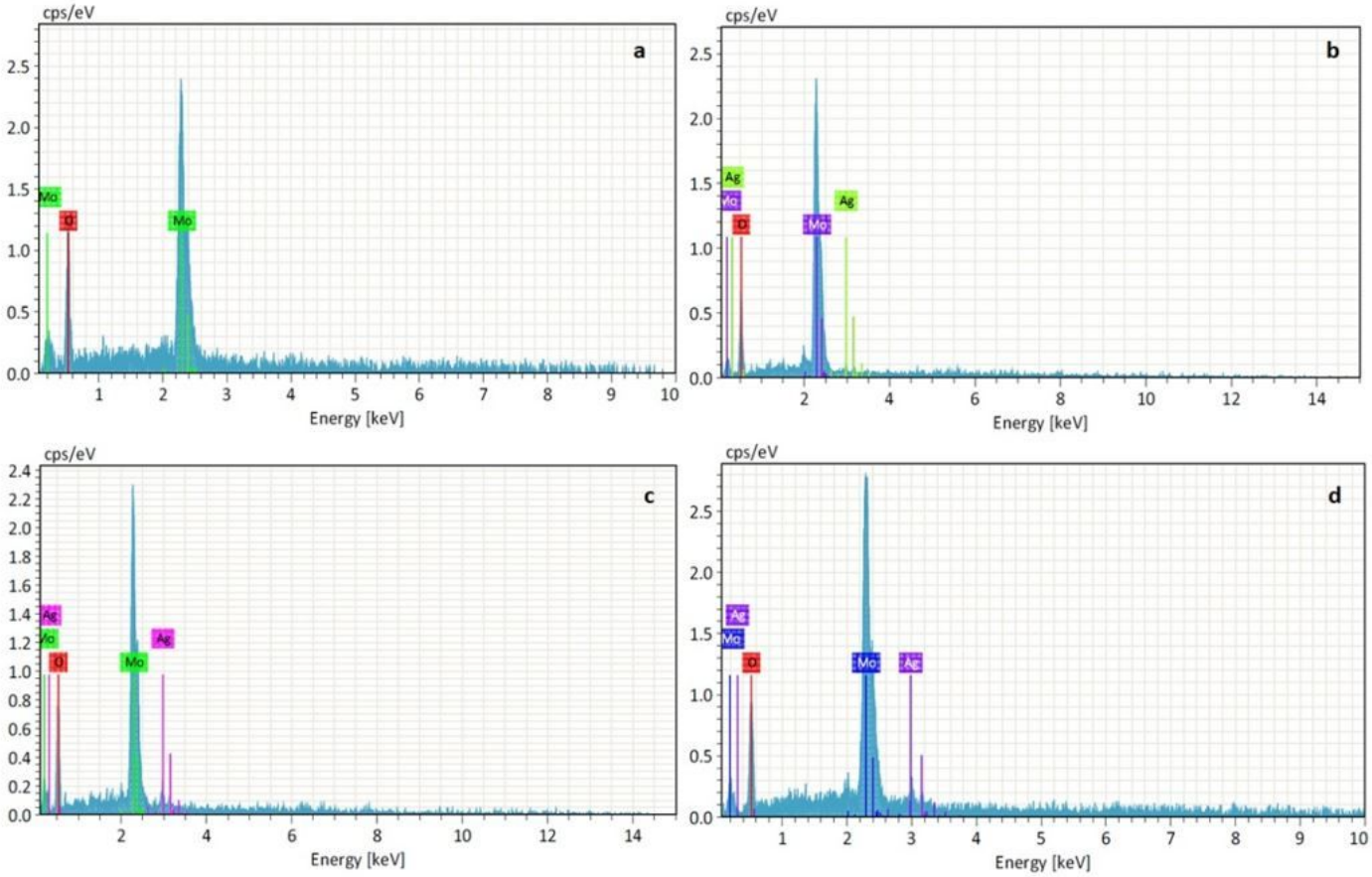

Figure 3

EDX spectra of MoO3 and Ag doped MoO3 nanoparticles (a) M, (b) 1AM, (c) 3AM and (d) 5AM

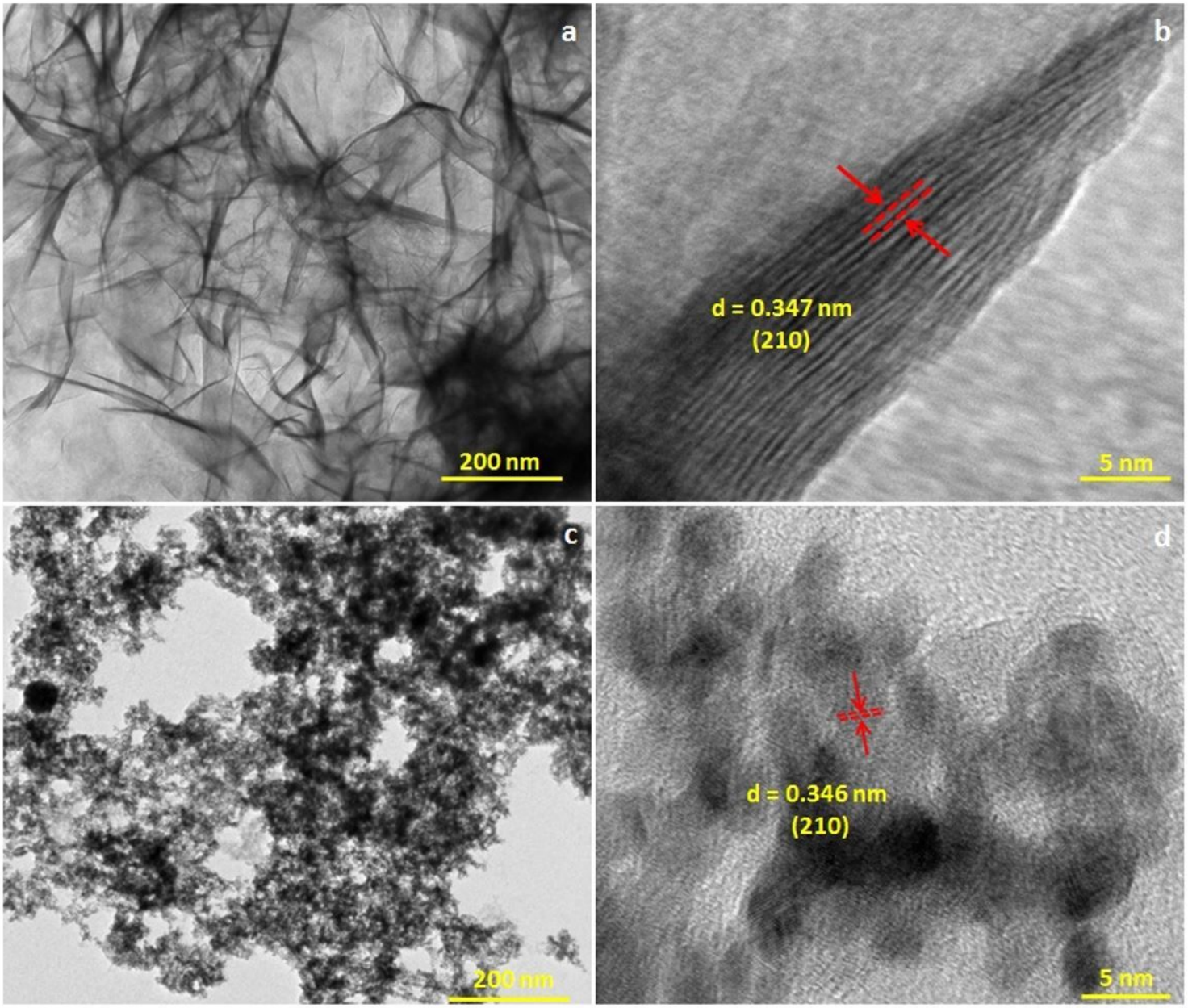

Figure 4

HRTEM images of (a,b) h-MoO3, and (c,d) 5% Ag doped MoO3 nanoparticles

MoO_3.

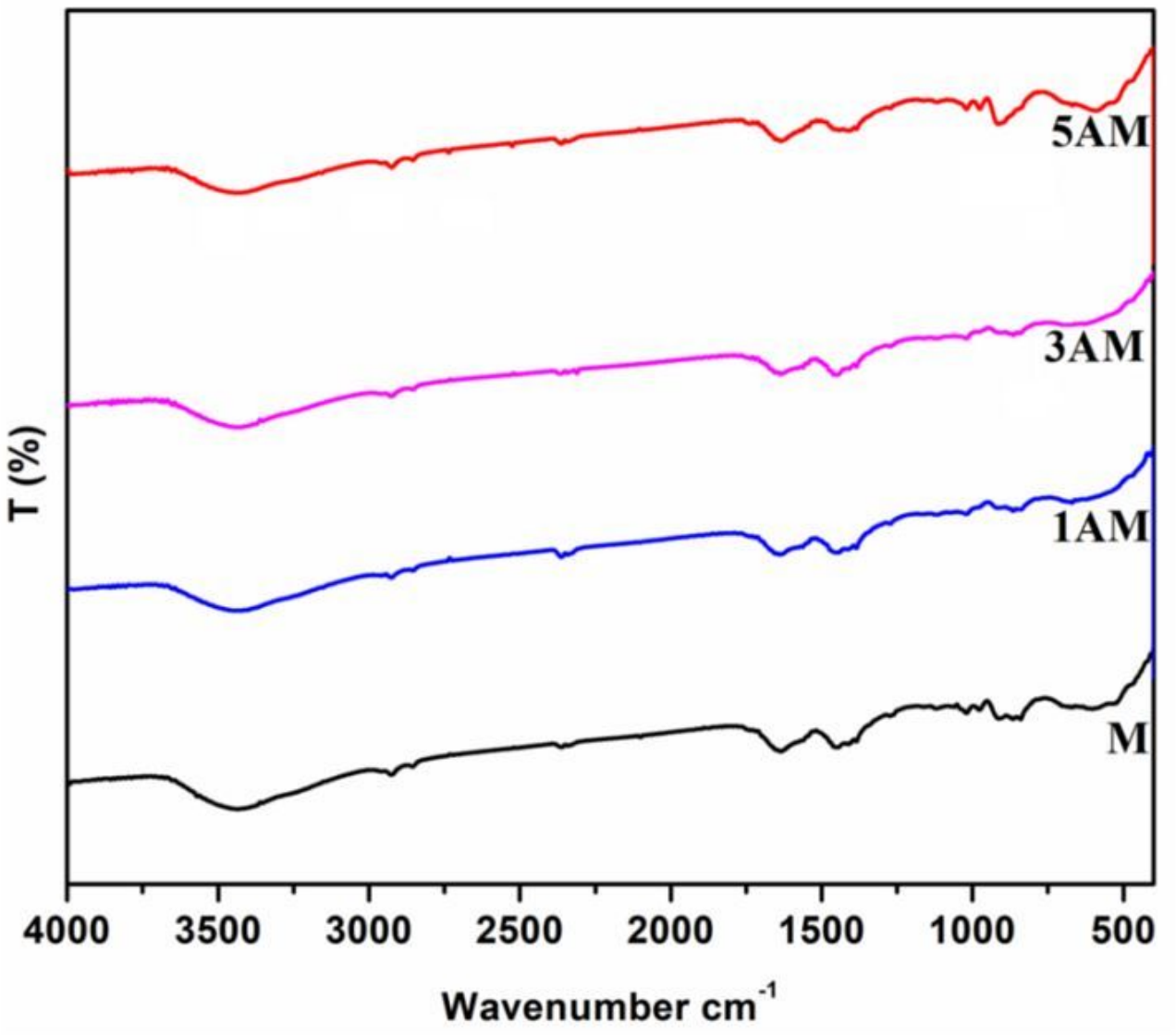

Figure 5

FTIR spectra of MoO3 and Ag doped MoO3 nanoparticles

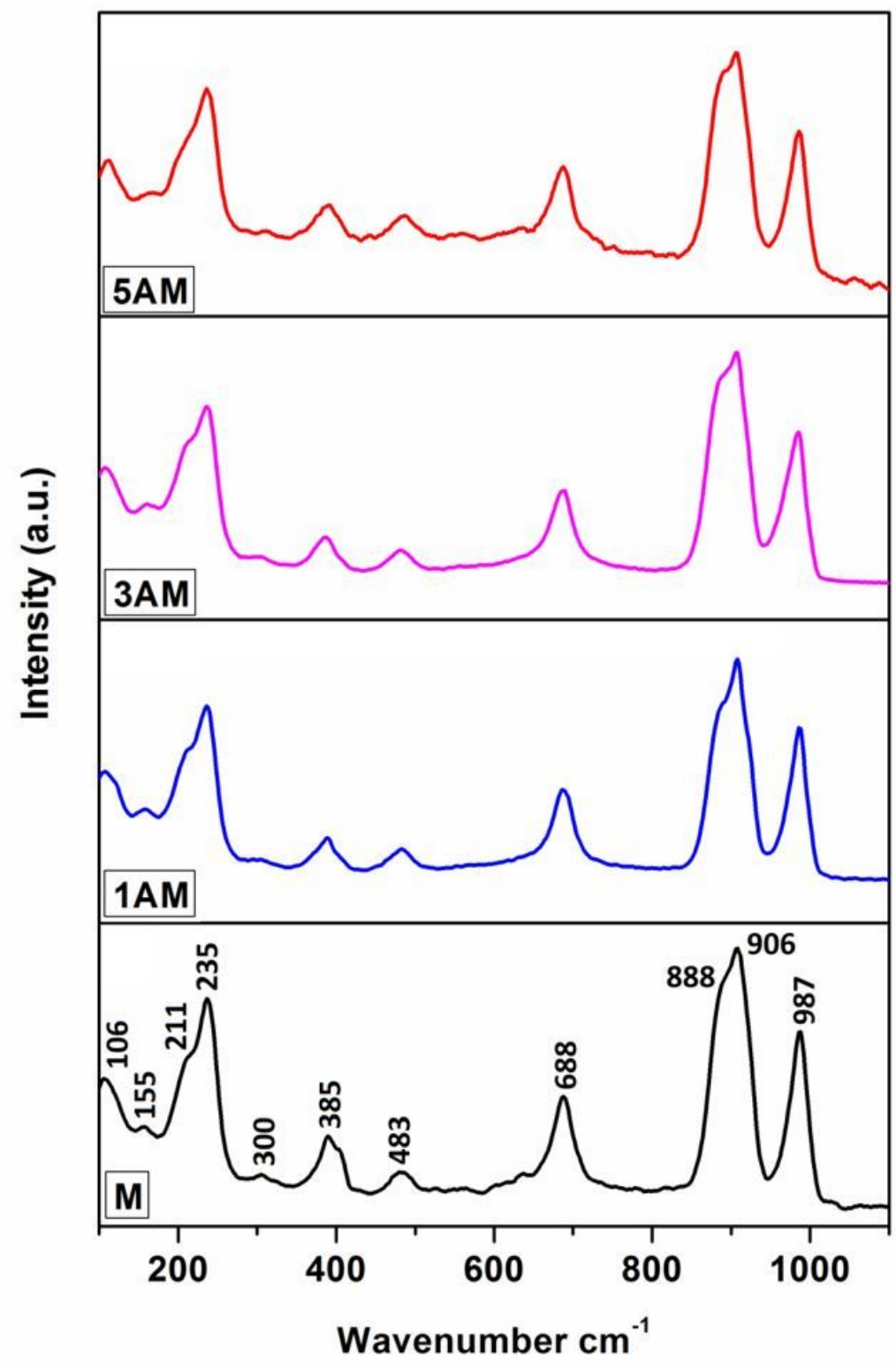

Figure 6

Raman spectra of MoO3 and Ag doped MoO3 nanoparticles

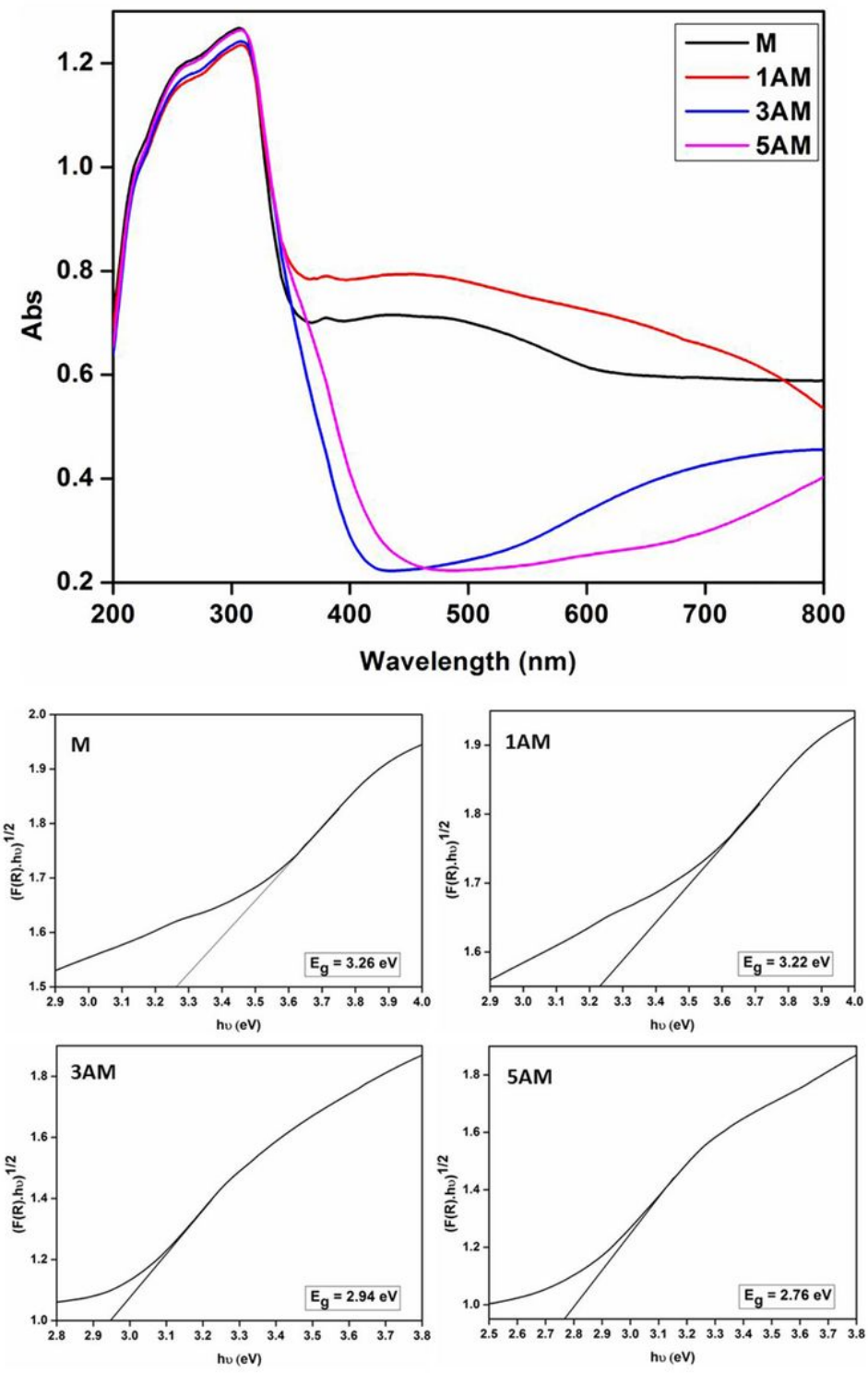

Figure 7

a Absorbance spectra of MoO3 and Ag doped MoO3 nanoparticles. b Band gap calculation using Kubelka–Munk (K–M) function for MoO3 and Ag doped h-MoO3 nanoparticles.

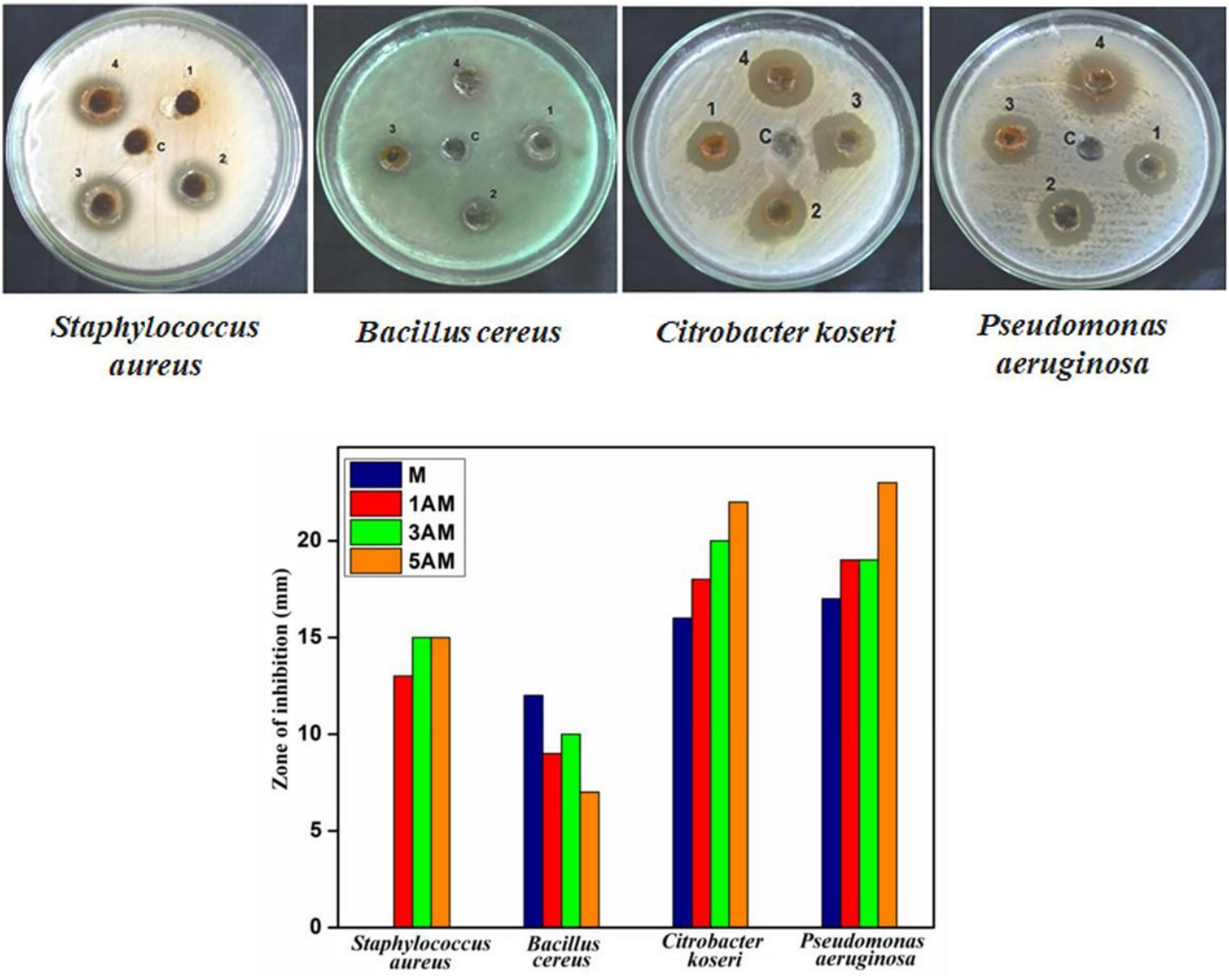

Figure 8

a. Antimicrobial properties of NPs against various bacterial strains. b. Zone of inhibition for bacterial growth by h-MoO3 and Ag doped h-MoO3 nanoparticles

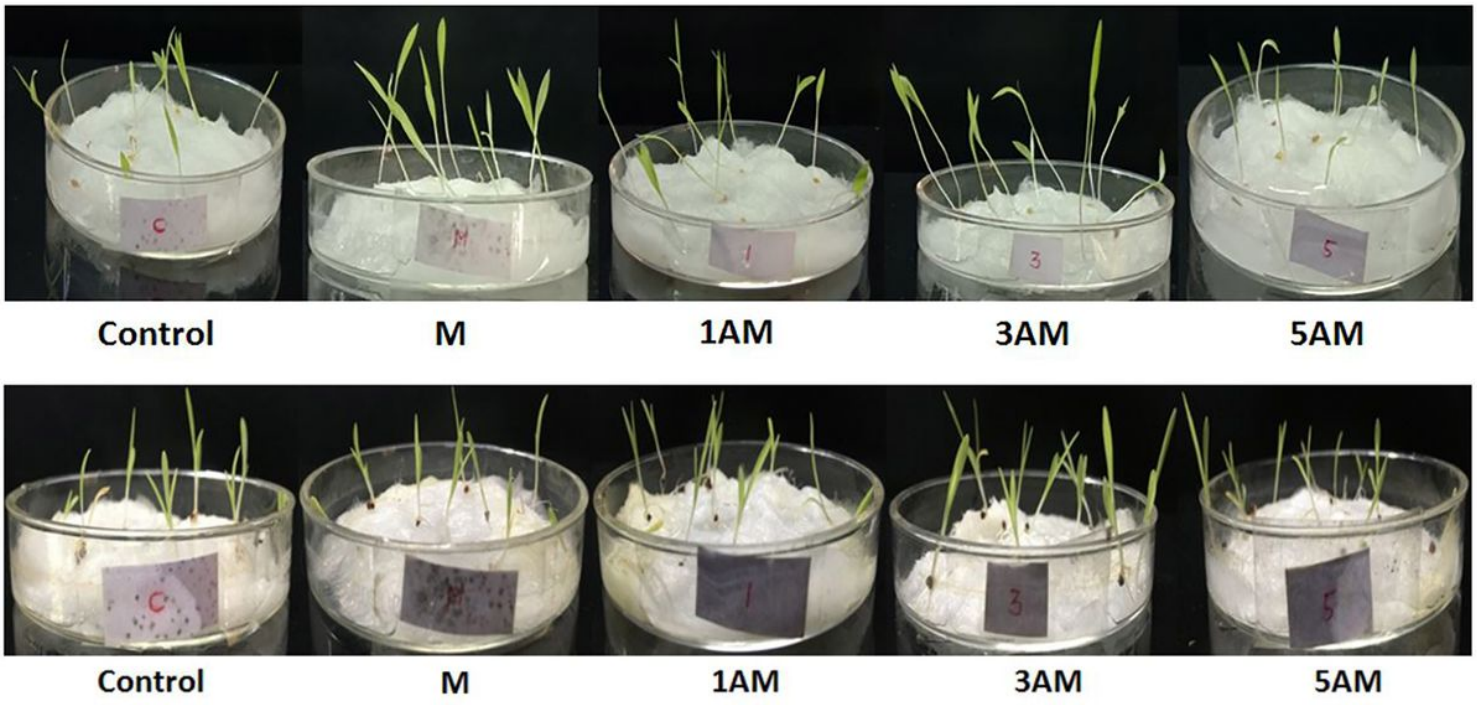

Figure 9

a. Germination of Foxtail millet seeds by MoO3 and Ag doped MoO3 nanoparticles. b. Germination of Finger millet seeds by MoO3 and Ag doped MoO3 nanoparticles

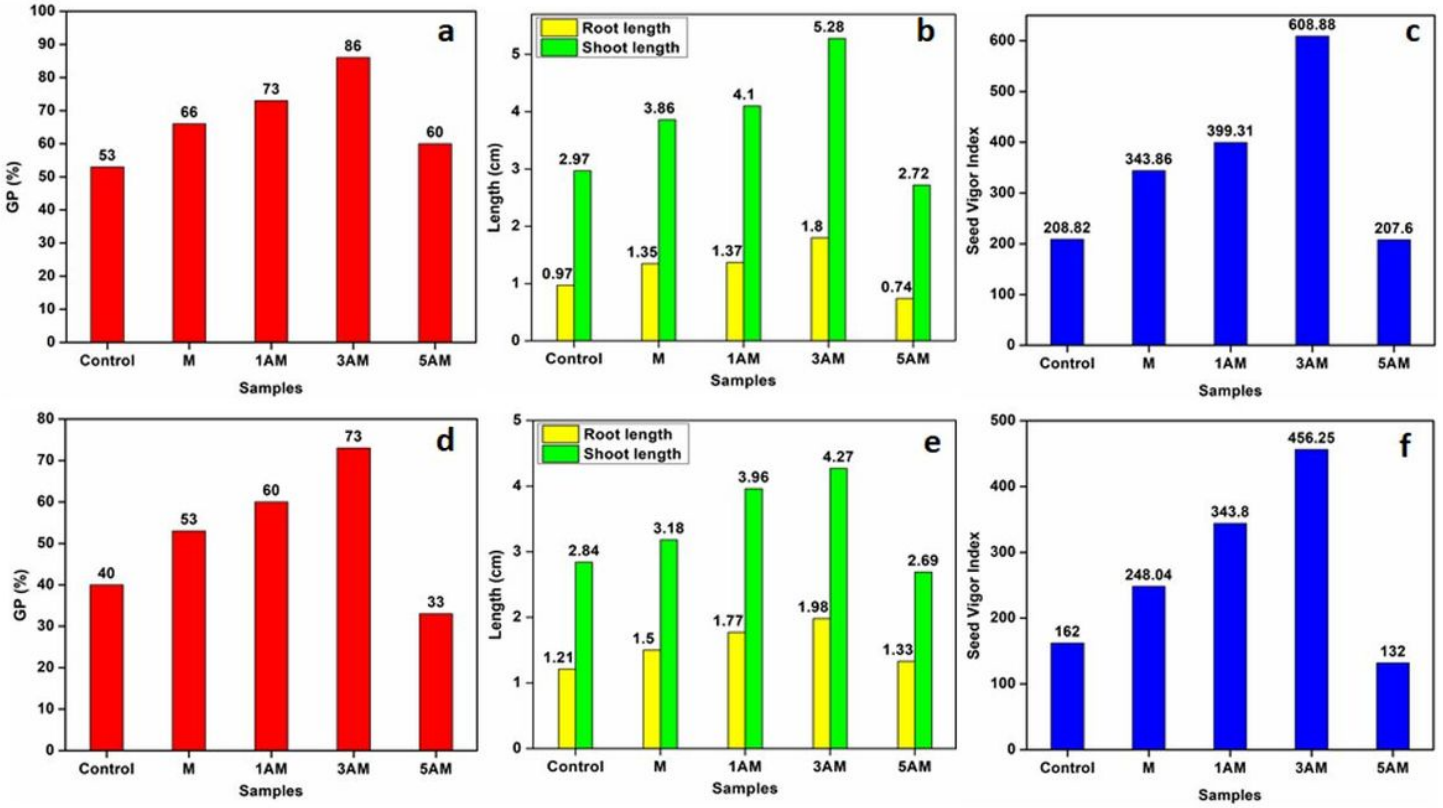

Figure 10

(a,d) Germination percentage, (b,e) Root and shoot length, and (c,f) seed vigour index of foxtail millet and finger millet seeds respectively treated with MoO3 and Ag doped MoO3 nanoparticles